J. Fluid Mech. (2010), *vol.* 652, *pp.* 75–103.

doi:10.1017/S0022112010000017

Large-eddy simulation of a buoyant plume in uniform and stably stratified environments

B. J. DEVENISH†, G. G. ROONEY AND D. J. THOMSON

Met Office, FitzRoy Road, Exeter EX1 3PB, UK

(Received 22 October 2008; revised 22 December 2009; accepted 1 January 2010; first published online 9 April 2010)

We consider large-eddy simulation (LES) of buoyant plumes in uniform and stably stratified environments. We show that in the former case the results agree well with the simple plume model of Morton, Taylor & Turner (*Proc. R. Soc. Lond.* A, vol. 234, 1956, p. 1). In particular, we calculate an entrainment constant which is consistent with laboratory and field measurements and find no significant difference between the radial spreading rates of vertical velocity and buoyancy. In a stably stratified environment, the LES plume shows better agreement with Morton *et al.* (1956) below the level at which the buoyancy first vanishes than above this level. Above the level of neutral buoyancy, the LES plume is characterized by an ascending core of negative buoyancy surrounded by a descending annulus of positive buoyancy. We compare the LES data with the model of Bloomfield & Kerr (*J. Fluid Mech.*, vol. 424, 2000, p. 197), which explicitly accounts for these coherent motions. The model exhibits many qualitative aspects of the LES plume and quantitative agreement can be improved by adjusting the downward volume flux relative to the upward volume flux in a manner consistent with the LES plume. This simple adjustment, along with revised values of the entrainment constants, represents the combined effects of an overturning region at the top of the plume (where a fluid element reverses direction), 'plume-top' entrainment (whereby the plume entrains ambient fluid above the plume) as well as lateral entrainment and detrainment processes (both external and internal) occurring above the top of the model plume.

1. Introduction

Buoyant plumes occur in a wide variety of natural and man-made situations. Despite their obvious complexity, they have been amenable to relatively simple theoretical models. Morton *et al.* (1956, hereafter referred to as MTT) proposed a model for plumes in a Boussinesq environment in terms of the mass, momentum and buoyancy fluxes by making two important assumptions. The first assumption is that the entrainment of ambient fluid by the plume occurs at a rate proportional to the mean vertical velocity such that the ratio of the mean inward horizontal velocity at the plume boundary and the mean vertical velocity of the plume is constant throughout the depth of the plume. The second assumption is that the mean vertical velocity and buoyancy profiles are self-similar with height. For plumes in a uniform (neutrally stratified) environment, the resulting plume equations admit analytical solutions and for plumes in a stably stratified environment, numerical or approximate analytical solutions can be obtained. These models have been remarkably successful

† Email address for correspondence: ben.devenish@metoffice.gov.uk

in describing buoyant plumes and detailed reviews can be found in e.g. List (1982), Turner (1986) and Gupta (1993).

The aim of this paper is to compare plumes generated by large-eddy simulations (LES) with the mathematical plume theory described above. The success of this theory provides a stringent test of LES and, in this context, it is perhaps somewhat surprising that there have been relatively few studies of purely buoyant plumes using LES, particularly when compared with jets and forced plumes (e.g. Akselvoll & Moin 1996; Le Ribault, Sarkar & Stanley 1999; Zhou, Luo & Williams 2001). Among the LES studies of buoyant plumes are Nieuwstadt & de Valk (1987), Bastiaans *et al.* (2000), Abdalla *et al.* (2007), Yan (2007) and Pham, Plourde & Doan (2007). With the exception of Nieuwstadt & de Valk (1987), who considered a line plume in a convective atmospheric boundary layer, all the studies are restricted to a uniform environment. Bastiaans *et al.* (2000) performed LES of a line source and Yan (2007) and Pham *et al.* (2007) considered an effectively axisymmetric source. In this study, we restrict attention to the latter configuration. Direct numerical simulations (DNS) of the Navier–Stokes equations for purely buoyant plumes have been conducted by Pham *et al.* (2007) and Plourde *et al.* (2008). The former authors make a systematic comparison of their DNS results with different subgrid models for LES. We use the Smagorinsky–Lilly model to account for dissipation by the smallest eddies in our LES. Although Pham *et al.* (2007) note some discrepancies between the classical Smagorinsky model and DNS, since our main interest is in comparing mean field statistics derived from the LES with the mathematical plume theory, we do not consider other subgrid models. In addition to dissipation, LES also accounts explicitly for the perturbation pressure gradient. These aspects, which are absent from the MTT model, coupled with the fact that the filter separating the resolved and unresolved scales lies within the inertial subrange of turbulence (and thus allows a wide range of eddies to be resolved), all contribute to much richer behaviour than is possible in the MTT model. Thus, LES in turn points to the limitations of the mathematical plume theory. We shall show that while the mathematical plume theory agrees well with LES in a uniform environment, in a stably stratified environment this is only partially true. In particular, we quantify the differences between the LES plume and the mathematical theory.

The paper is organized as follows. In § 2, we present a summary of plume theory for an axisymmetric Boussinesq plume from a point source, and in § 3 we give a brief outline of the numerical solution of the Boussinesq equations in LES. In this study, we assume the validity of the Boussinesq approximation: in practice, this does not lead to accurate predictions for the near-source region, but since our main interest is the well-developed region sufficiently far above the source, we do not consider this to be a significant limitation. The LES results are presented in § 4 for a uniform environment and in § 5 for a stably stratified environment.

2. Summary of plume theory

Equations for the volume, momentum and buoyancy fluxes for a plume from a point source can be derived from the Navier–Stokes equations in their Boussinesq form (with suitable approximations) and the continuity equation (see e.g. Rooney & Linden 1996; Linden 2000). The governing equation for the volume flux is given by

$$\frac{\mathrm{d}V}{\mathrm{d}z} = -2\pi r u|_{r=\infty}, \tag{2.1}$$

where V is the volume flux, r is the radial coordinate, z is the vertical coordinate and u is the radial component of velocity evaluated far from the plume. The governing equation for the momentum flux is given by

$$\frac{\mathrm{d}M}{\mathrm{d}z} = 2\pi \int_0^\infty g'(r,z) r \,\mathrm{d}r, \tag{2.2}$$

where M is the momentum flux, $g'(r,z) = g(\rho_a(z) - \rho(r,z))/\rho_0$ is the reduced gravity or buoyancy of the plume, $\rho(r,z)$ is its density, $\rho_a(z)$ is the ambient density, ρ_0 is a reference density and g is the gravitational acceleration. The governing equation for the buoyancy flux is given by

$$\frac{\mathrm{d}F}{\mathrm{d}z} = -N^2 V, \tag{2.3}$$

where F is the buoyancy flux and $N = ((g/\rho_0)\mathrm{d}\rho_a/\mathrm{d}z)^{1/2}$ is the buoyancy frequency. The fluxes V, M and F are defined respectively by

$$V = \int_0^\infty 2\pi w(r,z) r \,\mathrm{d}r, \quad M = \int_0^\infty 2\pi w^2(r,z) r \,\mathrm{d}r, \quad F = \int_0^\infty 2\pi w(r,z) g'(r,z) r \,\mathrm{d}r, \tag{2.4}$$

where $w(r,z)$ is the vertical velocity of the plume. Provided that both w and g' have the same r-dependence, the right-hand side of (2.2) can be expressed as FV/M for arbitrary profiles of w and g' (Linden 2000, § 3.5).

It is commonplace to express the fluxes and plume equations in terms of an average (across the plume) vertical velocity, $\overline{w}(z)$, and reduced gravity, $\overline{g'}(z)$, along with a radius, $b(z)$, which are defined by

$$V = \pi b^2 \overline{w}, \quad M = \pi b^2 \overline{w}^2, \quad F = \pi b^2 \overline{w}\,\overline{g'}.$$

Provided g' is proportional to w as r varies at a given z, the right-hand side of (2.2) can be expressed as $\pi b^2 \overline{g'}$. The plume variables $\overline{w}(z)$ and $\overline{g'}(z)$ would follow naturally from the definitions of V, M and F in the case that w and g' are assumed to have a top-hat profile (as was originally done by MTT for a uniform environment) and this motivates the more general definition of $\overline{w}(z)$ and $\overline{g'}(z)$. In reality, the time-averaged cross-plume profiles of the vertical velocity and reduced gravity are more appropriately described by Gaussian profiles (Turner 1973, § 6.1):

$$w(r,z) = \hat{w}(z) \exp\left(-\frac{r^2}{b_w^2}\right), \quad g'(r,z) = \hat{g}'(z) \exp\left(-\frac{r^2}{b_g^2}\right), \tag{2.5}$$

where $\hat{w}$ is the centreline vertical velocity, $\hat{g}'$ is the centreline reduced gravity and b_w and b_g are typical radii associated with the widths of w and g', respectively, at a given z. The centreline variables can be expressed in terms of the plume variables via (2.4):

$$\overline{w} = \frac{1}{2}\hat{w}, \quad b = b_w\sqrt{2}, \quad \overline{g'} = \frac{1}{1 + b_w^2/b_g^2}\hat{g}'. \tag{2.6}$$

Equation (2.5) allows for different spreading rates of w and g'; however, with $b_w = b_g$ the right-hand side of (2.2) can be expressed as FV/M or $\pi b^2 \overline{g'}$ as discussed above. In terms of the fluxes, (2.2) becomes

$$\frac{\mathrm{d}M}{\mathrm{d}z} = \frac{FV}{M}. \tag{2.7}$$

The plume equations (2.1)–(2.3) are commonly closed by means of the (Taylor) entrainment assumption, which states that the horizontal inflow velocity at the plume

boundary i.e. the entrainment velocity, u_e, is proportional to the vertical velocity of the plume, that is, $u_e = \alpha \overline{w}$ where α is the entrainment constant. In a quiescent environment, the inflow velocity at the plume boundary is equal to its far-field value, namely, $bu_e = -ru_{r=\infty}$ (since physically we require $\mathrm{d}V/\mathrm{d}z > 0$). The volume flux equation, (2.1), then becomes

$$\frac{\mathrm{d}V}{\mathrm{d}z} = 2\alpha\pi^{1/2}M^{1/2}. \tag{2.8}$$

In a uniform environment, the plume equations admit similarity solutions for $\overline{w}$, b and $\overline{g'}$ (Turner 1973, § 6.1):

$$\overline{w} = \frac{5}{6\pi^{1/3}\alpha}\left(\frac{9}{10}\alpha F\right)^{1/3} z^{-1/3}, \quad b = \frac{6}{5}\alpha z, \quad \overline{g'} = \frac{5}{6\pi^{2/3}\alpha}\left(\frac{9}{10}\alpha\right)^{-1/3} F^{2/3} z^{-5/3}. \tag{2.9}$$

3. Large-eddy simulation

The three-dimensional Boussinesq equations for an incompressible fluid form the basis of the large-eddy model. The evolution of the resolved, or filtered, velocity, $\boldsymbol{u}$, is governed by

$$\frac{\partial \boldsymbol{u}}{\partial t} + \boldsymbol{u}\cdot\nabla\boldsymbol{u} = -\frac{1}{\rho_0}\nabla p + B\boldsymbol{k} + \nabla\cdot\boldsymbol{\sigma}, \quad \nabla\cdot\boldsymbol{u} = 0$$

where p is the pressure perturbation about the hydrostatic pressure and $\boldsymbol{k}$ is the unit vector in the vertical direction. The buoyancy is given by $B = g(T(\boldsymbol{x},t) - T_0)/T_0$ where T is the instantaneous (potential) temperature at time t and position $\boldsymbol{x}$ and T_0 is a reference temperature. The evolution of T is given by

$$\frac{\partial T}{\partial t} + \boldsymbol{u}\cdot\nabla T = \nabla\cdot\boldsymbol{Q}.$$

The stress tensor, $\boldsymbol{\sigma}$, and the heat flux, $\boldsymbol{Q}$, represent the influence of the subgrid-scale (unresolved) terms. The Smagorinsky–Lilly model is used to approximate the subgrid terms in which the stress tensor takes the form $\sigma_{ij} = 2\nu_T S_{ij}$, where $2S_{ij} = \partial u_i/\partial x_j + \partial u_j/\partial x_i$ and $i, j = 1, \ldots, 3$. The subgrid eddy viscosity is given by $\nu_T = \lambda^2 S f_m(Ri)$, where λ is the mixing length, $S = (2S_{ij}S_{ij})^{1/2}$ and f_m is a function of the Richardson number, $Ri = (1/S^2)\partial B/\partial z$, used to describe the stability of turbulent stratified flows. The form of f_m reflects the observation that turbulence persists for $Ri \lesssim 1$ and subsides for $Ri \gtrsim 1$ (see e.g. Pasquill & Smith 1983, § 2.3). The mixing length is given by $1/\lambda^2 = 1/\lambda_0^2 + 1/(k(z+z_0))^2$ where z_0 is the roughness length, $k = 0.4$ is the von Kármán constant and $\lambda_0 = C_s\Delta x$ (as in the standard Smagorinsky model) where Δx is the horizontal grid spacing and $C_s = 0.23$ is the Smagorinsky coefficient. The heat flux, $\boldsymbol{Q} = \kappa\nabla T$, where κ is the scalar (eddy) diffusivity and $\kappa = \lambda^2 S f_s(Ri)$ where f_s has a similar functional form to f_m. For further details see e.g. Mason (1989).

The momentum equations are solved using a centred-difference method based on Piacsek & Williams (1970). The evolution equation for the temperature is solved using a total variation diminishing (TVD) method (Leonard, Lock & MacVean 1996). The Poisson equation for the pressure is solved using a fast Fourier transform. Periodic boundary conditions are imposed on the lateral boundaries and a sufficiently large domain is chosen so that the periodicity has little effect on the plume over the duration of the simulation. No-slip and free-slip boundary conditions are imposed on the lower and upper boundaries, respectively, of the domain. The surface stress

Simulation	N/N_{max}	F_0/F_{min}	$b_0/F_0^{1/4}N^{-3/4}$	z_{eq}	z_{final}	z_{max}	N_z	$\Delta z/b_0$	H/b_0	z_{max}/R
S1	0.25	1	0.18	$15.9b_0$	$20b_0$	$24.6b_0$	80	0.5	40	0.49
S2	0.5	100	0.1	$30.7b_0$	$40b_0$	$47.2b_0$	140	0.5	70	0.81
S3	0.75	100	0.13	$22.7b_0$	$30b_0$	$34.7b_0$	120	0.5	60	0.7
S4	1	100	0.16	$17.7b_0$	$20b_0$	$29.3b_0$	100	0.5	50	0.59
S5	1	20	0.25	$10.5b_0$	$14b_0$	$17.5b_0$	100	0.3	30	0.35
S6	1	10	0.29	$8.21b_0$	$10.5b_0$	$13.0b_0$	100	0.25	25	0.26
S7	1	1	0.52	$3.79b_0$	$3.75b_0$	$6.6b_0$	100	0.2	20	0.13

TABLE 1. The details of the plume simulations in a stably stratified environment: N is the buoyancy frequency; F_0 is the initial surface buoyancy flux; b_0 is the source radius; z_{eq} is the equilibrium level; z_{final} is the final rise height; z_{max} is the maximum plume height; N_z is the number of vertical grid points; Δz is the vertical grid spacing; R denotes half the domain width and equals $50b_0$ for all cases except S2 for which it is $60b_0$. The number of horizontal grid points is 200 in each direction except for S2 where it is 240 with a horizontal extent of $120b_0$.

is determined using Monin–Obukhov similarity arguments (see e.g. Pasquill & Smith 1983, § 2.2) and the top of the domain is stress free. We added a small random perturbation of the ambient temperature in the lowest 5 % of the domain in order to help initiate a turbulent flow.

We specify a uniform non-zero heat flux in a circular source of radius b_0 in the centre of the lower boundary and zero heat flux outside this region. We use a finite source since the LES subgrid model cannot model a point source accurately. With sufficiently high resolution, this source is captured reasonably well with Cartesian coordinates. Unless otherwise stated, we use 200 grid points in each horizontal direction with a grid spacing of $\Delta x/b_0 = 0.5$ giving a horizontal extent of $100b_0$. We found that this resolution was sufficient to give good agreement with the observed plume generated by the explosion and fire at the Buncefield oil depot (Hertfordshire, UK) in December 2005 (Devenish & Edwards 2009). One purpose of this study is to establish how well the results of a simulation with this resolution agree with the predictions of § 2.

For a plume in a uniform environment we use 100 grid points in the vertical direction which gives a vertical grid spacing of $\Delta z/b_0 = 0.5$ and a domain height of $50b_0$. Newtonian damping towards the initial state (see e.g. Kantha & Clayson 2000, p. 228) in the top 20 % of the domain is used to ensure that, in this case, the plume does not impinge on the top of the LES domain. The maximum rise height of the plume, z_{max}, is approximately $40b_0$, which ensures that there is a region in which the plume becomes fully developed sufficiently far above the source that a meaningful comparison with the plume theory of § 2 can be made. Except on the first grid point above the surface, the resolved buoyancy flux is approximately conserved up to the level where the Newtonian damping takes effect. For plumes in a stably stratified environment, we consider a range of constant N values and initial buoyancy fluxes, F_0, which are listed in table 1. Here, N_{max} is typical of stable atmospheric conditions.

Although we are concerned with the simulation of a buoyant plume in an unbounded domain, we are in effect modelling a buoyant plume in a confined region. The latter has been studied both theoretically and experimentally by Baines & Turner (1969). They considered an initially uniform environment which is stabilized over time by the redistribution of warmer, or lighter, fluid by the plume. They argued that, in order to avoid a large-scale circulation, the stabilizing buoyancy force in the

region of detrainment at the top of the plume must be larger than the inertial force of the plume. This in turn places a restriction on the aspect ratio, $H/R \lesssim 1$, where H is the height and πR^2 is the cross-sectional area of the confined region. Manins (1979) strengthened this condition to $H^2/R^2 \ll 1$ in order to avoid large vertical accelerations in the fluid outside the plume, and experimental evidence for a line plume (Manins 1973) suggests that $H/R \lesssim 0.8$ is sufficient in practice. In an externally imposed stably stratified environment, the ratio z_{max}/R, where z_{max} is the maximum plume height, plays the role of H/R with the domain height chosen to be sufficiently high that the plume does not impinge on the top of the domain prior to coming to rest as a result of the stable stratification. The values of z_{max}/R for a range of simulations are shown in table 1. It will be seen that the condition $z_{max}/R \lesssim 0.8$ is satisfied in all cases thus ensuring that our results are not compromised by the finite domain size. In practice, we find that $z_{max}/R \lesssim 0.8$ does not need to be strictly satisfied with, for example, a modified simulation S2 with 200 grid points in each horizontal direction and a horizontal extent of $100b_0$, and for which $z_{max}/R \approx 0.95$, giving similar results to S2. For the plume in a uniform environment, $z_{max}/R \approx 0.8$ (due to the Newtonian damping). Although the condition $H/R \lesssim 1$ precludes the formation of a large-scale circulation, it does not prevent a slow change in the environmental temperature profile. However, the LES data samples are taken before such changes have a significant impact.

Figure 1 shows a series of instantaneous contour plots of the concentration of an arbitrary scalar field emitted from the source in order to visualize the plume. The simulation is of a typical plume in a stably stratified environment (S4). The time scale, τ, is defined as the maximum height of the plume divided by the maximum centreline velocity of the plume in its (quasi-)steady state. At the beginning of the simulation, the plume extends well above its steady-state maximum height; initially the ambient fluid is undisturbed (except for the random perturbation near the surface) with the result that the plume entrains at a lower rate than in its steady state. By the time the simulation reaches a steady state (figures 1*c* and 1*d*), the ambient fluid has been disturbed sufficiently that there is a degree of turbulence which increases the entrainment rate (and hence reduces the height of the plume).

Once the plume reaches a steady state, the plume statistics are calculated over a sufficiently long sample period such that fluctuations in the statistics are small. Statistics from several sample periods of 10τ each are calculated. Unless indicated otherwise, only time-averaged statistics from the plume in its steady state are presented below. Centreline statistics are calculated along the geometric centre of the domain and are denoted by a hat. We term fluxes that are calculated by integrating the instantaneous variables over a circle centred on the source and averaged over the sample period the 'total resolved' fluxes and we term 'mean' fluxes those fluxes that are calculated by integrating the time-averaged variables. Unless indicated otherwise, all the statistics are computed from the resolved variables so that the fluxes include contributions from the resolved fluctuations as well as the mean flow.

Figure 2 shows the centreline resolved and subgrid vertical velocities, respectively $\hat{w}$ and $\hat{w}_{SG}$, with the latter estimated as $w_{SG}^2 = 2\lambda^2 S^2/(3a^2)$ where $a^2 = 0.23$ is the stress-energy ratio. It is clear that, except very close to the surface and near the top of the plume, the energy of the plume is dominated by the resolved motions. Figure 3 shows the total (resolved and subgrid) buoyancy flux, the resolved mean buoyancy flux, the resolved fluctuating buoyancy flux and the subgrid buoyancy flux. As with the energy of the plume, the buoyancy flux is dominated by the resolved motions

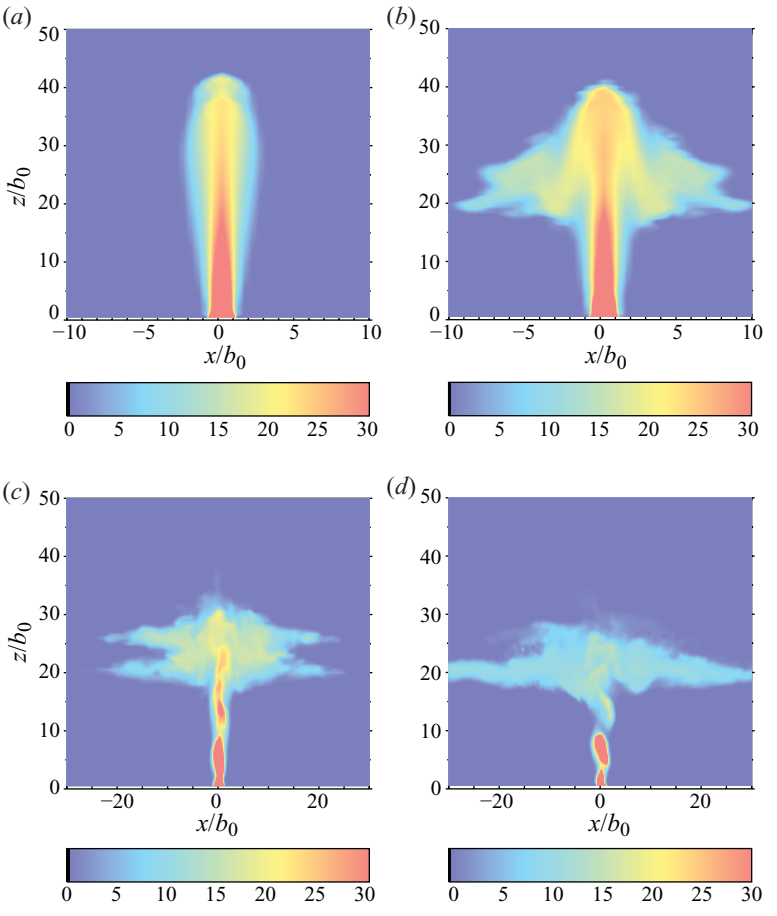

FIGURE 1. Contour plots of the instantaneous scalar concentration (arbitrary units) showing the evolution of plume S4: (*a*) $t = 2.5\tau$, (*b*) $t = 10\tau$, (*c*) $t = 30\tau$ and (*d*) $t = 60\tau$.

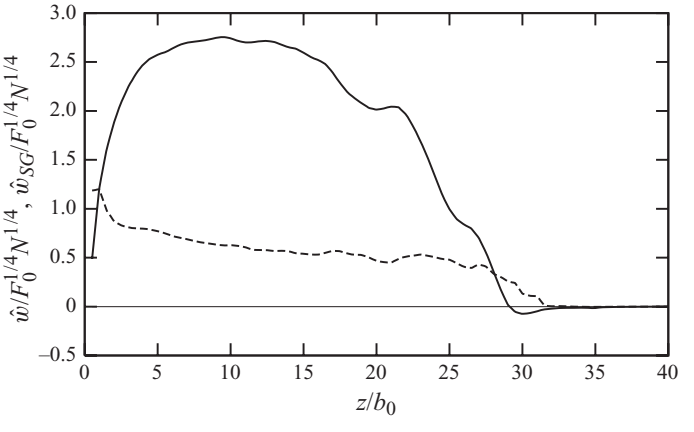

FIGURE 2. The resolved (solid) and subgrid (dashed) centreline vertical velocities for plume S4.

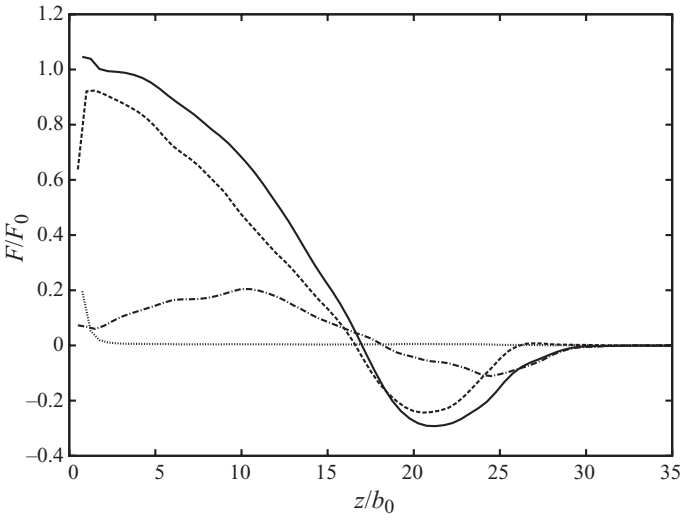

FIGURE 3. For plume S4, F represents the total (resolved and subgrid) buoyancy flux (solid), the resolved mean buoyancy flux (dashed), the resolved fluctuating buoyancy flux (dot-dashed) and the subgrid buoyancy flux (dotted).

except very close to the surface. The entrainment into the rising plume may, however, be less well resolved and hence more sensitive to the subgrid model.

To test the sensitivity of the plume statistics to the finite source size, we repeated simulation S4 with an initial radius $b_0' = b_0/2$, keeping the total surface heat flux as before, setting $\Delta x/b_0' = 0.5$ and using 400 grid points in each horizontal direction (so that the domain size remains the same). We found that the plume takes longer to reach a steady state but its statistics do not differ significantly from the equivalent simulation with the original value of b_0 and 200 grid points in each horizontal direction.

We also conducted some sensitivity tests to changes in the resolution. Increased horizontal resolution (keeping b_0 fixed) also results in a plume which takes longer to reach a steady state but whose statistics do not differ significantly from those of the original simulation (except near the source). Changes in the vertical resolution do not have a significant impact on either the time to reach a steady state or the steady-state plume statistics. The results of sensitivity tests for plumes in a stably stratified environment are shown in figure 13. It is clear that increased horizontal or vertical resolution does not have a significant impact on the buoyancy flux.

4. Uniform environment

Figure 4 shows the centreline values of the vertical velocity and the reduced gravity, $\hat{g}'$, of the LES plume in a uniform environment. It is readily seen that, above the region in which the plume is developing, $\hat{w}$ scales like $z^{-1/3}$ and $\hat{g}'$ scales like $z^{-5/3}$, as predicted by (2.9).

The plume theory of MTT assumes a point source, whereas we have used a circular source of finite size. This can be corrected for by using the virtual point source, z_{vs}, associated with the finite (physical) source. The determination of the virtual source in practice is complicated by the difficulty in defining it precisely (see Gupta 1993 and Hunt & Kaye 2001 for a discussion on the various approaches that have been

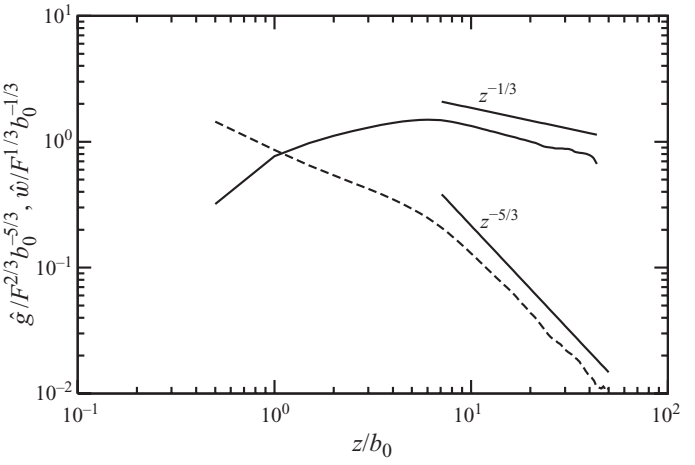

FIGURE 4. The centreline vertical velocity (solid) and reduced gravity (dashed) in a uniform environment.

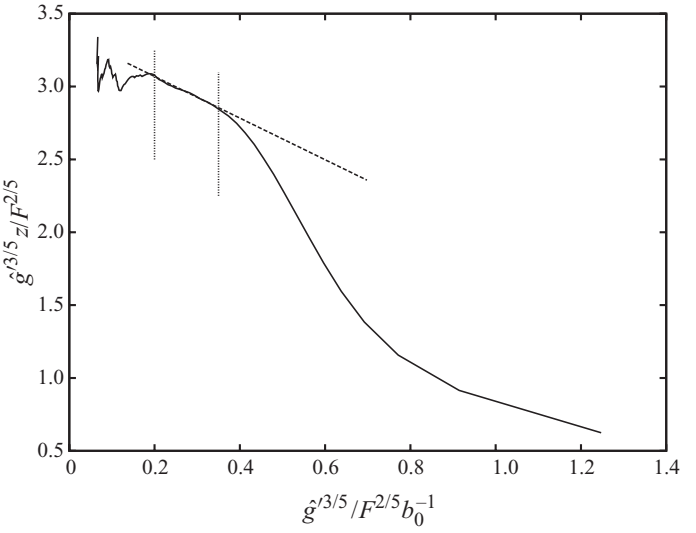

FIGURE 5. The centreline reduced gravity (solid) plotted as $\hat{g}'^{3/5}z$ versus $\hat{g}'^{3/5}$. The dashed line indicates the best linear fit between the two vertical lines.

used in the literature). Consequently, there are a number of ways of calculating the location of the virtual point source. We choose to calculate the virtual source from the centreline reduced gravity following George, Alpert & Tamanini (1977) (see also Hunt & Kaye 2001, § 1.1). Since $\overline{g'} \sim (z - z_{vs})^{-5/3}$, we get $\overline{g'}^{3/5}z = \overline{g'}^{3/5}z_{vs} + c$ where c is a constant and hence z_{vs} is given by the gradient of a plot of $\overline{g'}^{3/5}z$ against $\overline{g'}^{3/5}$. Figure 5 shows $\hat{g}'^{3/5}z$ against $\hat{g}'^{3/5}$ for the LES plume. The region in which the plume is well developed (where $\hat{g}' \sim z^{-5/3}$) corresponds to $0.2 \lesssim \hat{g}'^{3/5} \lesssim 0.35$; for $\hat{g}'^{3/5} \lesssim 0.2$ the plume is affected by the Newtonian damping and for $\hat{g}'^{3/5} \gtrsim 0.35$ the plume is affected by b_0. The gradient of a linear fit to the well-developed region gives a virtual source correction of $z_{vs} \approx -1.43b_0$.

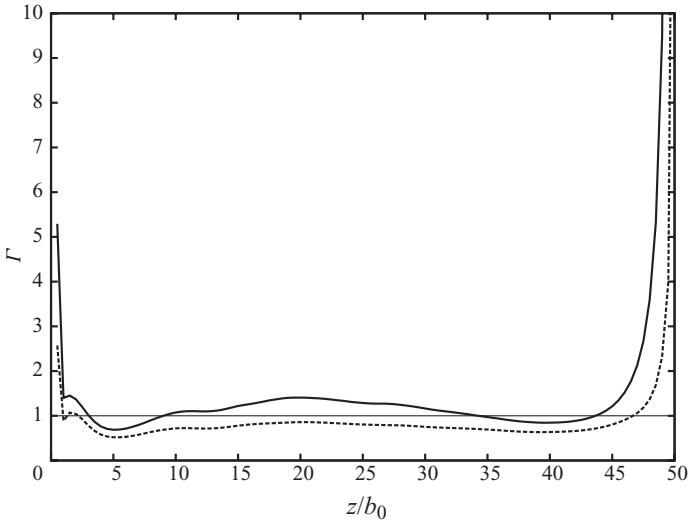

FIGURE 6. $\Gamma(z)$ evaluated from the mean fluxes (solid) and the total resolved fluxes (dashed) using $\alpha = 0.15$.

The value of the dimensionless quantity

$$\Gamma(z) = \frac{5FV^2(z)}{2^3\pi^{1/2}\alpha M^{5/2}(z)} \tag{4.1}$$

at the source, $\Gamma_0 = \Gamma(0)$, has been used to characterize forced plumes (Morton 1959; Hunt & Kaye 2001) and, more generally, $\Gamma(z)$ is proportional to a local Richardson number. (Note that the definition of Γ by Morton 1959 has been suitably rescaled for consistency with the plume equations of § 2.) For a purely buoyant plume $\Gamma(z) = 1$ for all $z > 0$ but it is not well defined at the source. In the limit $\Gamma_0 \to \infty$, Hunt & Kaye (2001) have shown that the virtual source coincides with the actual source. In the case that $\Gamma_0 = 1$, Morton (1959) has shown that the virtual source is located at $z_{vs} \approx -2.108 L_M$ where $L_M = 2^{-1}\pi^{-1/4}\alpha^{-1/2}M_0^{3/4}F^{-1/2}$ is a length scale characterizing the vertical distance over which a forced plume with initial momentum flux M_0 becomes a purely buoyant plume. For purely buoyant plumes with $M_0 = 0$, L_M is not an appropriate length scale and the source radius provides a more suitable length scale (Hunt & Kaye 2001).

Figure 6 shows (4.1) evaluated using the total resolved fluxes and the mean fluxes. (The value of $\alpha = 0.15$ is consistent with the LES data; see below.) With the exception of the near-source region (and close to the domain top), Γ calculated from the mean fluxes tends to be larger than unity whereas Γ calculated from the total fluxes tends to be smaller than unity. Although figure 6 shows that Γ is becoming large as z tends to zero, this cannot be regarded as conclusive due to the dominance of diffusion over advection close to the source and numerical difficulties in simulating the near-source region with limited resolution. Moreover, the plume equations of § 2 are not valid for the near-source region of the LES plume. Using Γ at the lowest grid point above the source, the virtual source correction of Hunt & Kaye (2001) (see (34) and figure 2 in that work) would give a value of z_{vs} which is close to the physical source. However, taking the average value of Γ in the region where the plume is well-developed (for which the plume equations are appropriate) gives a virtual source much farther below the physical source than that calculated above (even if we treat the effective source of the plume as the lowest point of the well-developed plume and subtract the difference

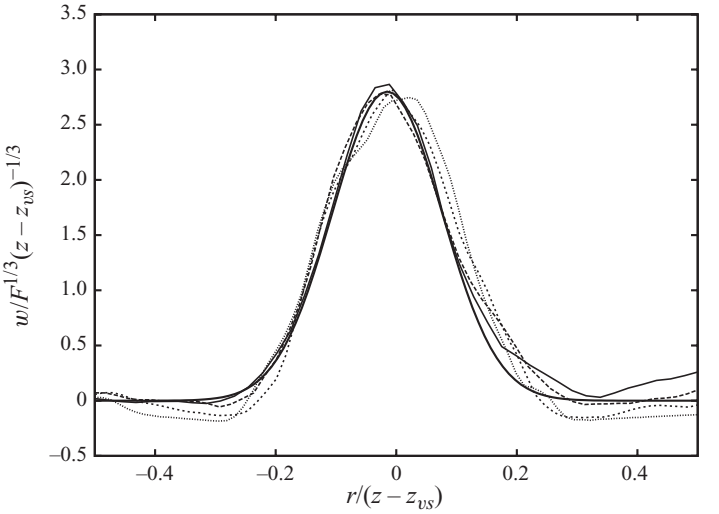

FIGURE 7. Cross-sections of the vertical velocity at $z/b_0 = 20$ (solid), $z/b_0 = 25$ (long dashed), $z/b_0 = 30$ (short dashed) and $z/b_0 = 35$ (dotted). The thick solid line is proportional to $\exp(-60(r/(z-z_{vs}))^2)$.

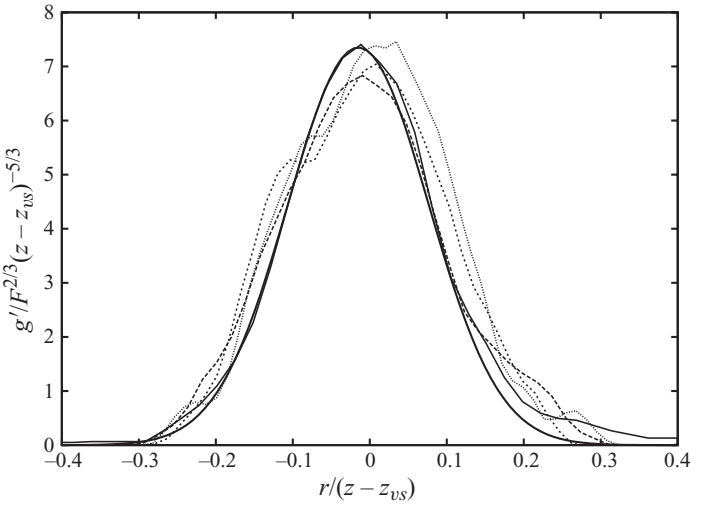

FIGURE 8. Cross-sections of the reduced gravity with the same key as in figure 7. The thick solid line is proportional to $\exp(-60(r/(z-z_{vs}))^2)$.

between this effective source and the physical source). The sensitivity of the virtual source location to the way in which it is determined means, of course, that any comparison of the LES results with plume theory is likely to be sensitive to the choice of virtual source. An alternative approach is to ask what value of z_{vs} is required for the LES results to agree with the predictions of § 2. For this reason and the ambiguity in the choice of Γ, we choose to use $z_{vs} = -1.43b_0$, calculated above, which ensures that $\overline{g'} \sim (z-z_{vs})^{-5/3}$ in the appropriate range of z. This leads to a value of α of the expected order of magnitude (see below).

Figures 7 and 8 show cross-sections of the mean vertical velocity and reduced gravity, respectively, at a number of different values of z/b_0. It is clear from

both figures that, within the region $20 \lesssim z/b_0 \lesssim 35$, the vertical velocity and reduced gravity are approximately self-similar with height. Moreover, both sets of profiles are reasonably well approximated by Gaussian profiles, $w \sim \exp(-\beta_1 r^2/(z-z_{vs})^2)$ and $g' \sim \exp(-\beta_2 r^2/(z-z_{vs})^2)$, with $\beta_1 = 60 \pm 10$ and $\beta_2 = 60 \pm 10$. Equating these profiles with (2.5), we see that b_w and b_g take the same value and so there is no difference in the radial spreading rates of w and g'. The ratio β_1/β_2 is within the range of experimental values listed in table 1 of Linden (2000): of the six experiments quoted, half calculated a value of β_1/β_2 less than unity and half a value that is greater than unity. These results also indicate that the plume radius grows linearly with z. Thus, we can use (2.6*b*) and (2.9*b*) to estimate a value of the entrainment constant $\alpha = 0.15 \pm 0.015$ that agrees well with the value determined from the LES plume of Abdalla *et al.* (2007), the experimental values listed by Linden (2000) and field measurements (e.g. Briggs 1984). We find that without the virtual source correction, the profiles of w and g' at the same values of z still collapse when scaled appropriately but with a slightly different spreading rate that results in a value of α that is approximately 15 % larger. This suggests that for the finite source used in this LES, the virtual origin correction has only a small effect on the plume statistics in the region where the plume is well developed.

5. Stably stratified environment

In a stably stratified environment, the density of a buoyant plume increases with height due to entrainment while that of the environment decreases with height. At some point, the density difference vanishes and above this height the buoyancy force acts on the plume to reduce its momentum and eventually bring it to rest. The plume then falls back down and, as it does so, it continues to entrain ambient fluid as well as interacting with the ascending plume. After the descending plume is brought to rest by the increasingly positive buoyancy, the plume then re-ascends and these oscillations continue until the plume finally comes to rest at its 'final rise height'. The result is that the final rise height may not be the same as the level at which the buoyancy first vanishes, the 'equilibrium level' (see also the discussion in MTT). Below the equilibrium level, a plume in a stably stratified environment behaves very much like a plume in a uniform environment. Indeed, as Briggs (1984) has noted, $1/N$ is the time scale to reach the equilibrium level and this time scale is independent of F_0. Thus, for times much less than $1/N$, the stratification should have little effect on the plume rise. The result is that below the equilibrium level the rate of entrainment can be assumed to be the same in both stably stratified and uniform environments.

We start this section by looking at how well the LES fluxes satisfy the plume equations of § 2 and thus how well justified are the assumptions that underlie them. In § 5.1 we compare the LES data with the numerical solution of the plume equations of § 2 and Briggs' (1975) approximate analytical solutions of these equations. As we find that neither captures the upper part of the plume accurately, in § 5.2 we consider the more sophisticated model of Bloomfield & Kerr (2000; hereafter referred to as BK2000) which is based on a model by McDougall (1981). This was originally developed for a turbulent fountain and we start by applying it directly (using the same values of the entrainment constants) to a purely buoyant plume.

In figures 9, 10 and 11, we plot the left-hand and right-hand sides of the buoyancy, momentum and volume equations, respectively, evaluated from the LES data for simulation S4. Figure 9 shows that the buoyancy equation (2.3) is approximately satisfied throughout the depth of the plume (with the exception of the near-source

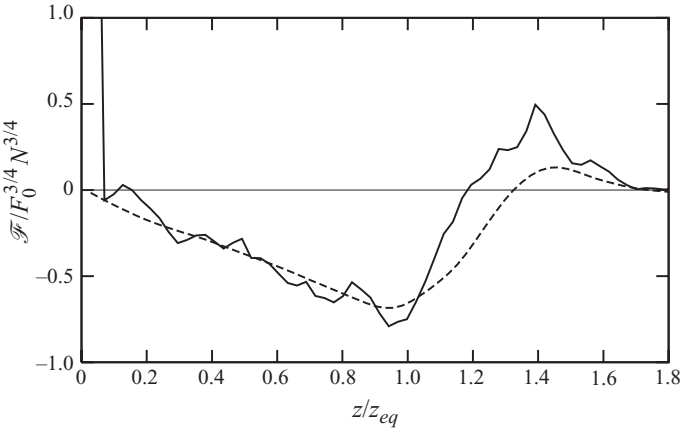

FIGURE 9. $\mathscr{F}$ represents the left-hand (solid) and right-hand (dashed) sides of (2.3) for plume S4.

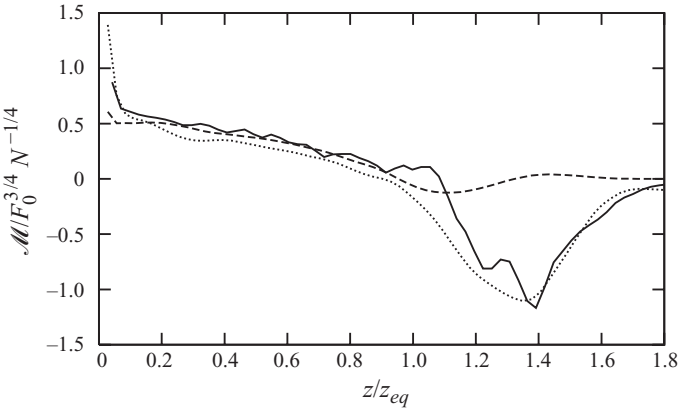

FIGURE 10. $\mathscr{M}$ represents the left-hand (solid) and right-hand sides of the momentum equation with the dotted line the right-hand side of (2.2) and the dashed line the right-hand side of (2.7).

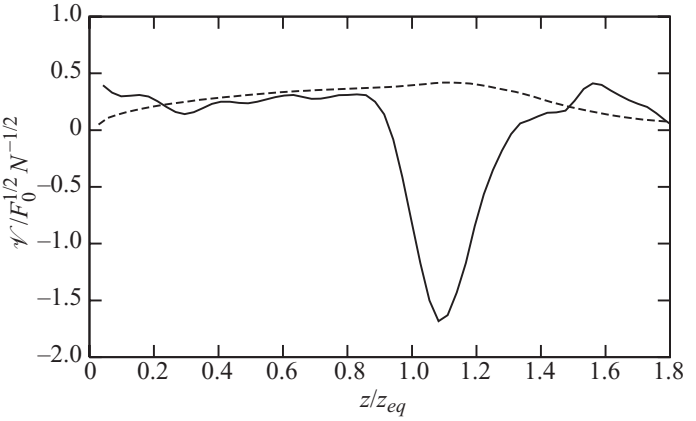

FIGURE 11. $\mathscr{V}$ represents the left-hand (solid) and right-hand (dashed) sides of (2.8) with $\alpha = 0.1$ for plume S4.

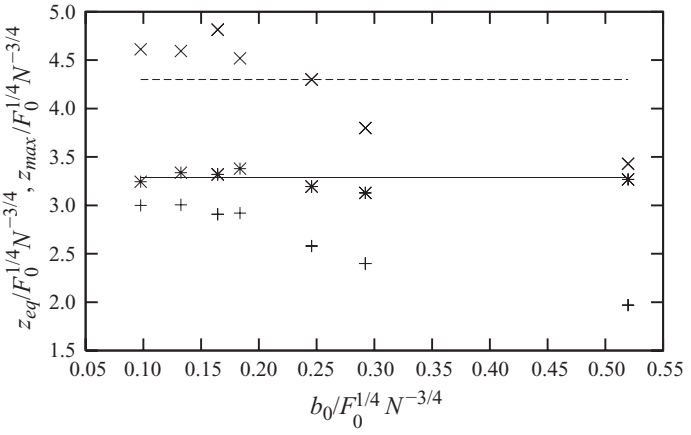

FIGURE 12. The LES z_{eq} (+) and z_{max} (×) for the simulations listed in table 1 as a function of $b_0/F_0^{1/4}N^{-3/4}$. The solid and dashed horizontal lines are (5.1a) and (5.1b), respectively, with $\alpha = 0.1$. The LES z_{eq} with the virtual source correction is indicated by (∗).

region). Figure 10 shows that the momentum equation is reasonably well satisfied throughout the depth of the plume when the right-hand side is evaluated as in (2.2). However, when the right-hand side of the momentum equation is evaluated as in (2.7), the two sides of the momentum equation only agree for $z \lesssim z_{eq}$, where z_{eq} is the equilibrium level. Figure 11 shows that the volume equation (2.8) (with $\alpha = 0.1$ for best fit) is reasonably well satisfied for $z \lesssim z_{eq}$ but not for $z \gtrsim z_{eq}$. These results lead us to make the following remarks: (i) the LES plume provides a reasonable solution of the buoyancy flux and momentum flux equations (provided the right-hand side of the latter is evaluated as in (2.2)) but not of the volume flux equation. This supports the assumptions leading to (2.2) and (2.3) such as the neglect of the radial pressure gradient in the plume equations (see e.g. Linden 2000, § 3.4) but raises questions about the validity of the entrainment assumption in the upper part of the plume; we will return to this point in § 5.2. We note that the momentum and buoyancy flux equations do not depend directly on α and, when re-formulated in terms of time, $t = \int \mathrm{d}z/\overline{w}$, become independent of the volume flux. This may explain why the LES satisfies (2.2) and (2.3) but not (2.8). (ii) The constituents of FV/M each depend on $\overline{w}$ whereas the integral on the right-hand side of (2.2) does not. When FV/M is calculated from the mean fluxes, the disagreement between the left and right-hand sides of (2.7) for $z \gtrsim z_{eq}$ remains and implies that, for $z \gtrsim z_{eq}$, the shapes of $\overline{w}$ and $\overline{g'}$ no longer have the same r-dependence; this will be demonstrated in figures 17 and 18. In § 5.2, we will show that the upper part of the plume is characterized by coherent upward and downward motion which provides an explanation for why the shapes of $\overline{w}$ and $\overline{g'}$ no longer have the same r-dependence in this region and why FV/M does not agree with the left-hand side of the momentum equation for $z \gtrsim z_{eq}$.

5.1. *Comparison of LES with the plume model of MTT*

From a numerical solution of (2.3), (2.7) and (2.8), the levels at which the buoyancy and vertical velocity vanish can be estimated as respectively (MTT)

$$z_{eq} \approx 1.04\alpha^{-1/2}F_0^{1/4}N^{-3/4}, \quad z_{max} \approx 1.36\alpha^{-1/2}F_0^{1/4}N^{-3/4}. \tag{5.1}$$

Figure 12 shows z_{eq} and z_{max} computed from the LES plumes for the simulations listed in table 1. The equilibrium height is taken to be the level at which $\hat{g}'$ vanishes

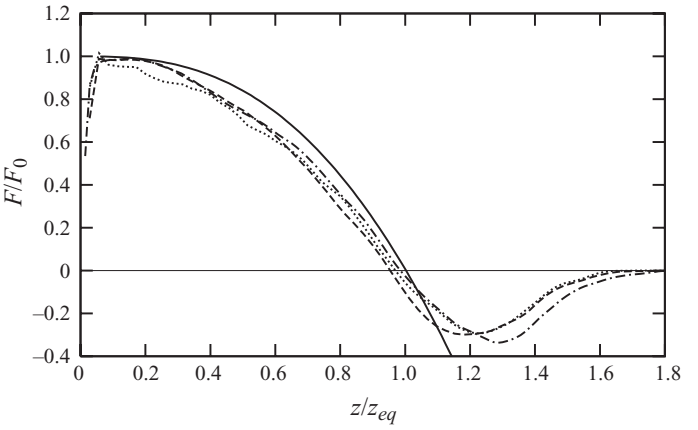

FIGURE 13. The MTT (solid) and LES buoyancy fluxes showing the effect of different resolutions. The dashed line represents the simulation S4, the dotted line represents the same simulation except with $\Delta x/b_0 = 0.25$ and 400 grid points in each horizontal direction and the dot-dashed line represents S4 except with $\Delta z/b_0 = 0.25$ and 200 vertical grid points.

and the maximum height of the plume is taken to be the level at which $\hat{w}$ vanishes. It is clear that the LES results and (5.1) agree better when b_0 is small relative to the length scale $F_0^{1/4}N^{-3/4}$; indeed we would expect the agreement to improve for smaller values of $b_0/F_0^{1/4}N^{-3/4}$ than we have considered here since we should recover a point source in the limit $b_0 \ll F_0^{1/4}N^{-3/4}$. As b_0 increases relative to $F_0^{1/4}N^{-3/4}$, the finite source size becomes more important; this can be corrected for using a virtual source correction. We choose to base the virtual source correction on z_{eq} and not z_{max} because we expect the MTT model to agree better up to, but not above, z_{eq}. Figure 12 suggests a virtual source correction of $2.5b_0$ and it can be seen that this results in better agreement with (5.1*a*). It is clear from figure 12 that since MTT overpredicts the LES z_{eq} and underpredicts the LES z_{max}, the virtual source correction cannot improve both simultaneously. Thus, correcting the LES z_{eq} results in a systematic underprediction of the LES z_{max} by MTT.

In order to gain more insight into how well the LES plumes agree with the MTT model, we compare the LES and MTT fluxes throughout the depth of the plume. Figure 13 shows the LES and MTT buoyancy fluxes and indicates that up to and including the equilibrium levels, the two fluxes agree reasonably well. (Note that z_{eq} is the appropriate value for either the LES or MTT plume.) The MTT value of z_{eq} is slightly larger than the LES z_{eq} which is consistent with figure 12. Figures 15, 16 and 23 show the buoyancy, momentum and volume fluxes, respectively, for the LES and MTT plumes scaled by F_0 and N (raised to the appropriate powers). The agreement between the LES and MTT fluxes is better for the buoyancy and momentum fluxes than that for the volume flux. In the context of what has already been discussed above regarding the plume equations (figures 9–11), this situation is perhaps not surprising.

Briggs (1975) introduced the 'unaltered volume flux' technique to derive an approximate analytical solution of the plume equations in a stably stratified environment. This method assumes that the volume flux is not significantly affected by the stratification and so can be approximated by the volume flux in a uniform environment. Substituting $V = \pi^{2/3}(6\alpha/5)(9\alpha/10)^{1/3}F_0^{1/3}z^{5/3}$ into (2.3) and (2.7), it is

straightforward to show that

$$F = F_0 - \frac{1}{2}\pi^{2/3}\left(\frac{9\alpha}{10}\right)^{4/3} F_0^{1/3} N^2 z^{8/3} \tag{5.2}$$

and

$$M^2 = \pi^{2/3}\left(\frac{9\alpha}{10}\right)^{4/3} F_0^{1/3} z^{8/3}\left(F_0 - \frac{1}{4}\pi^{2/3}\left(\frac{9\alpha}{10}\right)^{4/3} F_0^{1/3} N^2 z^{8/3}\right). \tag{5.3}$$

Equation (5.2) represents the first two terms in a series solution of (2.3) (with higher order terms proportional to $z^{8n/3}$ for $n = 2, 3, \ldots$). The next term in the series is given (numerically) by MTT and the full analytical solution can be found in Scase, Caulfield & Dalziel (2006). The latter authors found that the full series converges very rapidly implying that only the first two terms are significant. It follows from (5.2) and (5.3) that the equilibrium level and maximum rise height are given by

$$z_{eq} = 2^{3/8}\pi^{-1/4}\left(\frac{9\alpha}{10}\right)^{-1/2} F_0^{1/4} N^{-3/4}, \quad z_{max} = 2^{3/4}\pi^{-1/4}\left(\frac{9\alpha}{10}\right)^{-1/2} F_0^{1/4} N^{-3/4}. \tag{5.4}$$

The difference between the coefficients in (5.4*a*) and (5.1*a*) is approximately 1 % whereas the coefficient in (5.4*b*) is approximately 2.5 % smaller than that in (5.1*b*). The good agreement between (5.4) and (5.1), particularly for z_{eq}, provides justification for the unaltered volume flux technique. The fact that z_{eq} agrees better than z_{max} is consistent with the above arguments that the stratification does not play a significant role below z_{eq}. Above z_{eq}, the buoyancy becomes negative and the plume behaves like a jet. Furthermore, (5.2) becomes more negative than the buoyancy flux calculated from the numerical solution of the plume equations. Since jets spread out more rapidly than plumes (Turner 1973, § 6.1), it explains why the coefficient of (5.4*b*) is less than that of (5.1*b*). However, neither the numerical solution of the plume equations nor the approximate analytical solutions of Briggs' unaltered volume flux technique capture the LES z_{max} correctly.

Figure 14 shows the LES volume fluxes for a range of F_0 and N values along with the LES volume flux in a uniform environment. For $z \lesssim \min(15b_0, z_{eq})$, the volume fluxes in a stratified environment follow the volume flux in a uniform environment which would appear to justify the unaltered volume flux approximation. However, further examination of figure 14 shows that above $z/b_0 \approx 15$ but below the equilibrium levels of plumes S2 and S3, the volume fluxes of plumes S2 and S3 do not follow the volume flux in a uniform environment as might be expected. For all the stratified cases, the volume flux grows linearly until z_{eq} whereas the volume flux in a uniform environment grows linearly until $z/b_0 \approx 15$ and approximately like $z^{5/3}$ above this level. That the volume flux in a stratified environment does not scale like $z^{5/3}$ below the equilibrium level may be due to there being an insufficiently large separation between the region where the finite source affects the plume behaviour and the region where the stratification becomes important. With a much smaller source, we would expect such a separation to be achieved.

Figures 15 and 16 show that the LES data agree reasonably well with (5.2) and (5.3) which provides a better justification for the unaltered volume flux approximation. Note that, in this figure, we have restricted as far as possible the calculation of the fluxes to the upward core of the plume.

Briggs (1984) assumes that once the plume reaches its maximum height, it falls back down to its final rise or spreading height, z_{final}, with no further entrainment.

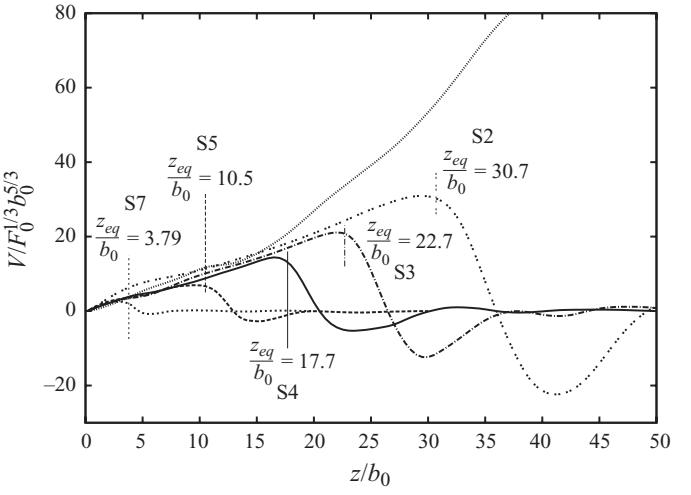

FIGURE 14. The volume flux for a range of F_0 and N values: simulation S2 for which $z_{eq} = 30.7b_0$, S3 for which $z_{eq} = 22.7b_0$, S4 for which $z_{eq} = 17.7b_0$, S5 for which $z_{eq} = 10.5b_0$ and S7 for which $z_{eq} = 3.79b_0$. The position of z_{eq} is marked by a vertical dash in the corresponding line type. The dotted line represents the volume flux for a plume in a uniform environment.

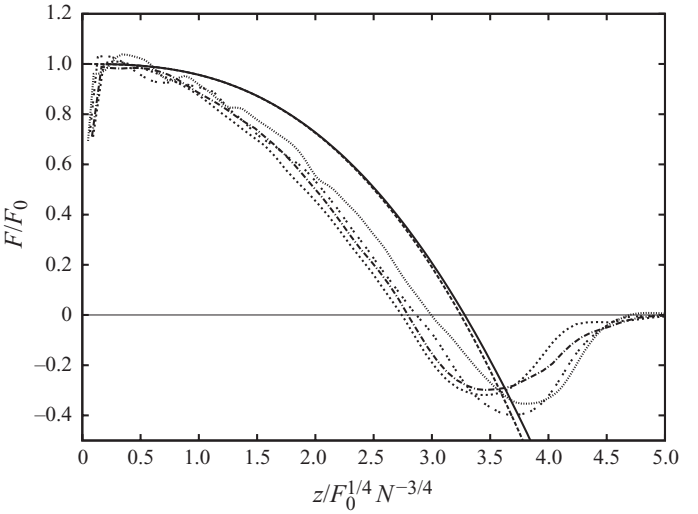

FIGURE 15. The LES buoyancy flux for a variety of F_0 and N values: simulation S1 (short dashed), S2 (dotted), S3 (two dashes) and S4 (dot-dashed). The long dashed line is the theoretical result (5.2) with $\alpha = 0.1$, and the solid line is the corresponding numerical solution of the MTT model with $\alpha = 0.1$.

This distance can be derived from (2.3) assuming that V remains constant over the interval z_{max} to z_{final} and using (5.2). Thus, we get

$$z_{final} = z_{max} + \left.\frac{F}{N^2 V}\right|_{z=z_{max}} = \frac{13}{16} z_{max}. \tag{5.5}$$

Using the LES z_{max}, table 1 indicates that, for $b_0 \ll F_0^{1/4} N^{-3/4}$, the LES z_{final} is, on average, $0.8z_{max}$ (in agreement with (5.5)) where z_{final} is estimated as the height of the

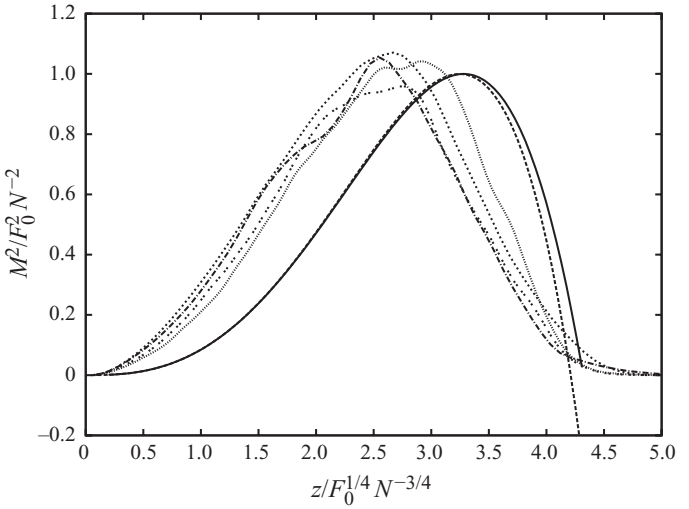

FIGURE 16. The same as figure 15 but for the square of the LES momentum flux. The long-dashed line represents the theoretical result (5.3) with $\alpha = 0.1$ and the solid line is the corresponding numerical solution of the MTT model with $\alpha = 0.1$.

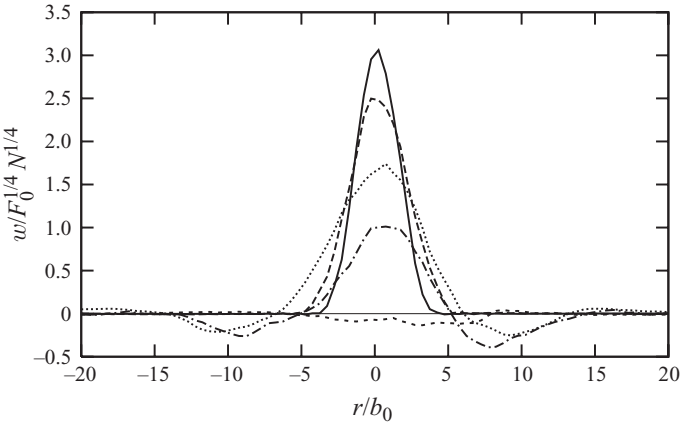

FIGURE 17. Cross-sections of mean w for plume S2 at $z/z_{eq} = 0.57$ (solid), $z/z_{eq} = 0.81$ (long dashed), $z/z_{eq} = 1.11$ (dotted), $z/z_{eq} = 1.35$ (dot-dashed) and $z/z_{eq} = 1.58$ (short dashed). Note that $z_{max} = 1.54 z_{eq}$.

maximum width of the plume. However, substituting (5.4*b*) into (5.5) gives a value of z_{final} which is considerably lower than the LES z_{final}. This suggests that, while the assumption of 'no further entrainment' may be a reasonable practical assumption, this may be the net result of a more complicated entrainment process.

5.2. *Comparison of LES with the plume model of BK2000*

Figure 17 shows the cross-section of the mean vertical velocity for plume S2 at increasing levels above the source. For $z = 0.57 z_{eq}$ and $z = 0.81 z_{eq}$, the vertical velocity is always positive whereas for $z = 1.11 z_{eq}$ and $z = 1.35 z_{eq}$ there is an annulus surrounding the central region where the plume is, on average, descending. Figure 18 shows corresponding profiles of g'. As z increases above z_{eq}, the buoyancy of the plume becomes increasingly negative, which leads to negative vertical velocities (since

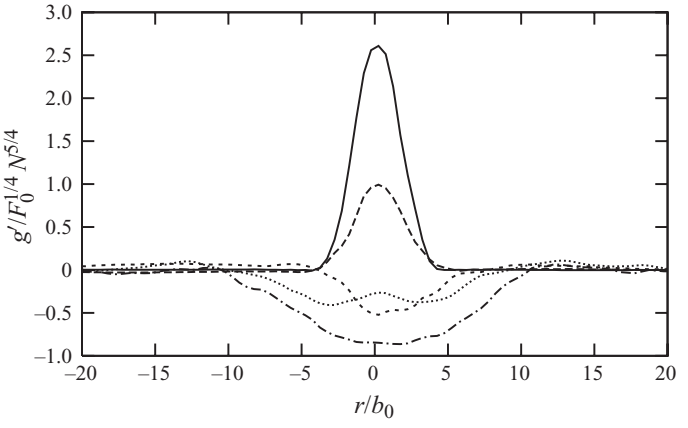

FIGURE 18. Cross-sections of mean g' for plume S2 at the same levels as in figure 17.

the right-hand side of (2.7) can be expressed as $F/\overline{w}$ and $M \geqslant 0$). The buoyancy of the descending shell of the plume eventually becomes positive and so there is an annulus of slightly positive buoyancy to the sides of the main plume for $z = 1.11z_{eq}$, which is larger than at $z = 1.35z_{eq}$. We note that although we have defined the top of the plume to be the level at which the centreline vertical velocity vanishes, there is a region above this level, as exemplified by $z = 1.58z_{eq}$, where an examination of the scalar concentration shows that there are still significant levels of plume fluid and which is characterized by negative vertical velocities. The corresponding cross-section of buoyancy shows that the buoyancy of the plume core is still negative but much less so than at $z = 1.35z_{eq}$. This is suggestive of entrainment of warmer ambient fluid above the plume; we will return to this point in § 5.3.

These results indicate that the region of the plume above z_{eq} is characterized by coherent concentric annuli consisting of either upward or downward motion. As demonstrated in the previous subsection, such behaviour is not captured by the simple plume model of MTT. BK2000 separate the upward (inner) and downward (outer) parts of the plume into two co-flowing plumes as shown schematically in figure 19. The model consists of six equations describing the evolution of (the square of) the momentum flux, the volume flux and the buoyancy flux for each of the two (upward and downward) plumes. Details of the numerical solution of the BK2000 model are given in the Appendix. BK2000 assume that there are three entrainment mechanisms with three entrainment velocities, $u_\alpha = \alpha\overline{w}_u$, $u_\beta = \beta\overline{w}_d$ and $u_\gamma = \gamma\overline{w}_d$ which respectively define the velocity of entrainment from the downward into the upward plume, from the upward into the downward plume and from the environment into the downward plume. In this section, we use the same values of the entrainment constants as BK2000 in the co-flowing region, namely, $\alpha = 0.085$, $\beta = 0.147$ and $\gamma = 0.147$. BK2000 consider two formulations of the buoyant body forces which lead to different forms of the governing equation for the momentum flux. In the first case, BK2000 assume that the pressure gradient is everywhere hydrostatic and that the surfaces of constant pressure remain horizontal throughout both the upward and downward plumes and the environment. In this case, the body force accelerating the upward plume depends only on the density difference between the upward plume and the environment so that the reduced gravity of the upward plume can be defined as $\overline{g'}_u = (g/\rho_0)(\rho_a(z) - \rho_u(z))$, where ρ_u is the density of the upward plume. In the second body-force formulation, BK2000 assume that the body force acting on the upward

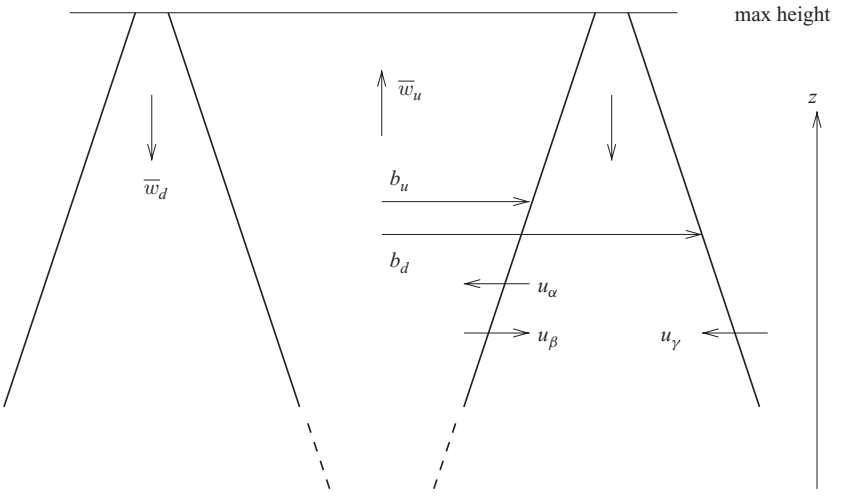

FIGURE 19. Schematic diagram showing the structure of the upper part of the plume with the inner, upward, plume and the outer, downward, plume. The radii of the upward and downward plumes are given by b_u and b_d, respectively, and $\overline{w}_u$ and $\overline{w}_d$ are the upward and downward vertical velocities, respectively. The entrainment velocities between the upward and downward velocities are u_α and u_β and that between the downward plume and the environment is u_γ.

plume is the local density difference between the upward and downward plumes, that is, $\overline{g'}_u + \overline{g'}_d$ where $\overline{g'}_d = (g/\rho_0)(\rho_d(z) - \rho_a(z))$ is the reduced gravity of the downward plume and ρ_d is its density. The downward body force changes correspondingly between the two formulations. We find only small differences between the two body-force formulations and as the first body force converges more readily we only present results for this case.

Figures 20 and 21 show the volume and momentum fluxes, respectively, for the BK2000 model. The model assumes that the limits of plume penetration are determined by the points at which the momentum flux goes to zero (and indeed the numerical solution breaks down beyond this point). Hence, the profiles of momentum flux always begin and end at approximately zero. The region in which the plume turns (from upward to downward motion) is not modelled but instead the fluxes are matched between the one-dimensional upward and downward plume models. This treatment leads to the abrupt cutoffs evident in the volume-flux profiles. The initial equilibrium and maximum rise heights are the same as the MTT model, namely (5.1*a*) and (5.1*b*) respectively. The final maximum rise height, z_{fmrh}, and the maximum downward penetration, z_{mdp}, shown schematically in figure 22 can be calculated from the BK2000 model. The final rise height, z_{final}, is calculated assuming that there is no further entrainment (see the Appendix for details). These heights can be expressed in terms of z_{eq} as given by (5.1*a*): $z_{fmrh} = 1.28 z_{eq}$, $z_{final} = 1.05 z_{eq}$ and $z_{mdp} = 0.94 z_{eq}$. Compared with the LES plumes in table 1, z_{fmrh} and z_{final} are smaller than z_{max} and z_{final}, respectively.

Figures 20 and 21 also show the (conditional) time-averaged LES volume and momentum fluxes conditioned on $w > 0$ or $w < 0$ for plume S2 (note that here w is the time-averaged vertical velocity). Both the downward volume and momentum fluxes become zero slightly below z_{eq}, indicating that the downward shell of the plume penetrates below z_{eq}. The level at which the fluxes become zero is approximately $0.9 z_{eq}$ compared with $0.94 z_{eq}$ predicted by the BK2000 model. In both the BK2000

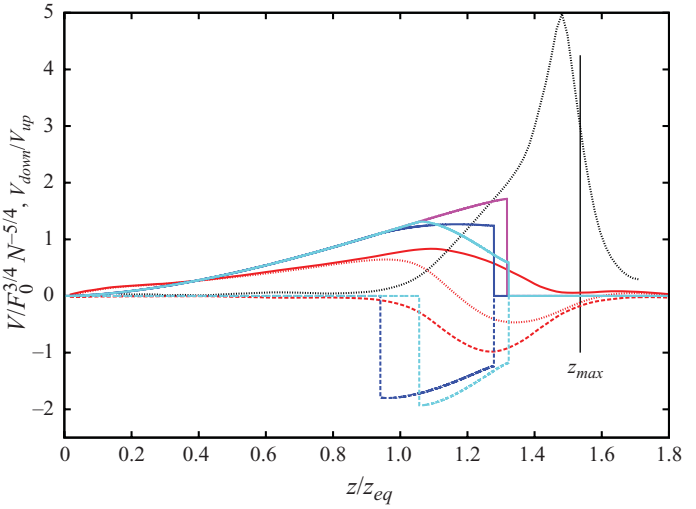

FIGURE 20. The upward (solid) and downward (dashed) volume fluxes: LES plume S2 (red); original BK2000 model with $\alpha = 0.085$, $\beta = 0.147$ and $\gamma = 0.147$ (blue); the revised BK2000 model with plume-top entrainment ($V_{down} = 2V_{up}$) and $\alpha = 0.05$, $\beta = 0.8$ and $\gamma = 0.01$ (cyan). The MTT volume flux with $\alpha = 0.1$ is shown by the purple line. The unconditional LES volume flux is shown by the dotted red line and the absolute ratio V_{down}/V_{up} is shown by the dotted black line. The position of the LES z_{max} relative to z_{eq} is marked by the vertical black line. The equilibrium value, z_{eq}, is the appropriate value for either the LES plume or the BK2000 and MTT models.

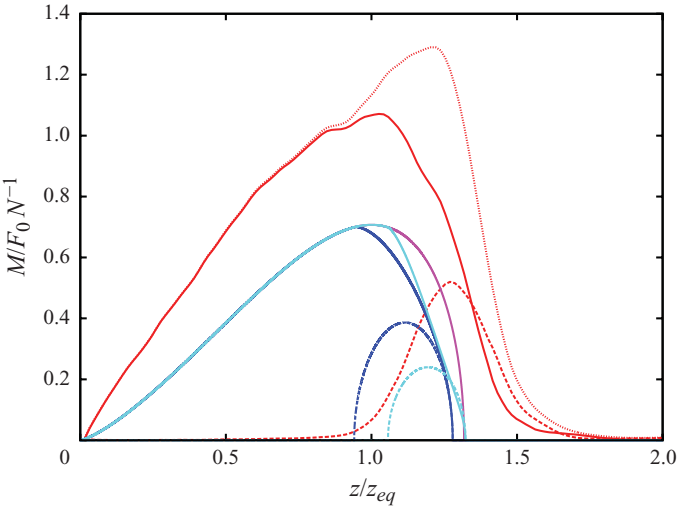

FIGURE 21. The same as figure 20 but for the momentum flux.

model and the LES data, the upward momentum flux is considerably larger than the downward momentum flux, and the position of the peak values is lower in the BK2000 model than that in the LES data.

5.3. *Plume-top entrainment*

It is evident from the LES results in figure 14 that, near the top of the plume, the volume flux becomes negative, which implies that the downward volume flux is greater

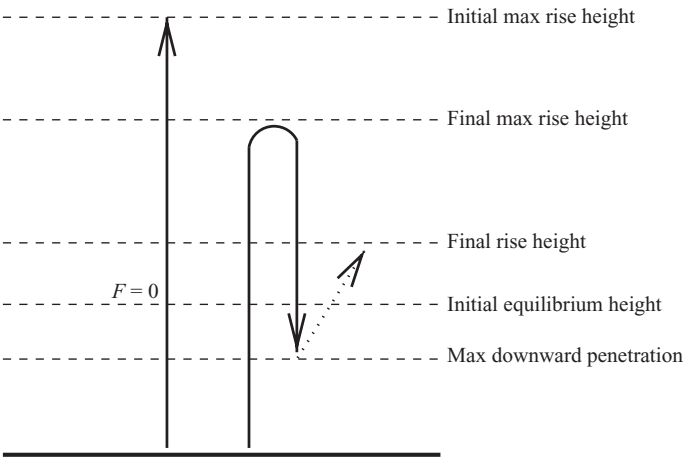

FIGURE 22. Schematic diagram showing the levels attained by the MTT plume (left) and BK2000 plume (right) as described in the text. The dotted-line arrow indicates the rise of the plume from z_{mdp} to its final rise height assuming no further entrainment.

than the upward flux. We also note that, as shown in figures 2 and 17, there is a region at the top of the plume in which the vertical velocity is negative. These results are indicative of 'plume-top entrainment', whereby the plume entrains ambient fluid from above the top of the plume, in the region in which the plume is overturning.

Plume-top entrainment has been extensively studied in a two-layer environment (see e.g. Cardoso & Woods 1993; Lin & Linden 2005) where the entrainment at the density interface is often characterized in terms of a Richardson number formed from the density difference across the interface and the plume similarity solution (Lin & Linden 2005). A pure plume from a point source in a stratified environment is characterized by two parameters: the initial buoyancy flux F_0 and the ambient buoyancy frequency N. It is clear that although these parameters are sufficient to non-dimensionalize the plume equations, no dimensionless group can be formed from them. The dimensionless equations describe a single problem with no parameter that can be varied independently and hence any data non-dimensionalized using F_0 and N should, in theory, collapse onto a single curve where b_0 is not important. Figures 15, 16 and 23 each show that the collapse to a single set of results occurs to a reasonable approximation for the buoyancy, momentum and volume fluxes throughout the depth of the plume (and indicates that, for the plumes shown in these figures, $b_0/F_0^{1/4}N^{-3/4}$ is sufficiently small for the collapse to be valid close to the source). We note that, for $z/(F_0^{1/4}N^{-3/4}) \gtrsim 4.5$, where the momentum and buoyancy fluxes vanish, the volume flux oscillates with a dimensionless wavelength and amplitude which appears to depend on N. A buoyant plume in a stratified environment generates gravity waves that radiate in all directions and whose properties depend on N. Since the fluxes are calculated by integrating over a fixed region, the volume flux only captures part of the gravity waves and hence appears to oscillate.

In the present problem, for the reasons given above, attempting to construct a Richardson number, Ri, from theoretical considerations yields a result that does not depend on F_0 or N, but which is a function of the entrainment constant alone. Turner (1973, § 7.1.1) makes an analogous point with reference to convection between horizontal plates: 'The Richardson number cannot enter here, because there is no externally imposed velocity, independent of the buoyancy forces'. That is, the single

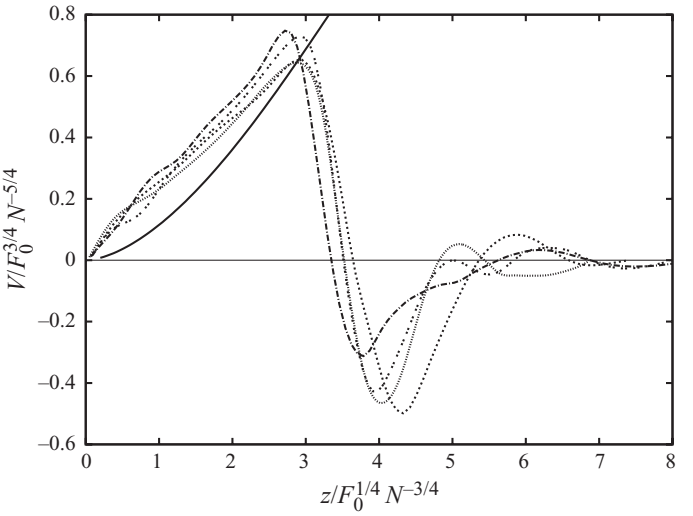

FIGURE 23. The volume flux for a range of F_0 and N values: simulation S1 (short dashed), S2 (dotted), S3 (two dashes) and S4 (dot-dashed). The solid line is the numerical solution of the MTT model with $\alpha = 0.1$.

problem allows only a single instance of entrainment behaviour. Some of these constraints are alluded to by Cardoso & Woods (1993), who studied a similar problem to that examined here but with time dependence arising from an environment of limited extent. To illustrate, using Briggs' solution, we may construct Ri using (5.2) and (5.3), taking the reduced gravity at the plume top, and the plume length and velocity scales at the equilibrium height:

$$\begin{aligned} Ri &\sim \frac{|g'(z_{max})|b(z_{eq})}{w^2(z_{eq})} \\ &= \frac{F(z_{max})}{V(z_{max})}\frac{V^3(z_{eq})}{\pi^{1/2}M^{5/2}(z_{eq})} \\ &= 2^{5/8}\frac{24}{15}\alpha \\ &\approx 2.47\alpha. \end{aligned}$$

Applying this value of Ri to the results of Lin & Linden (2005, figure 12) indicates that, in the two-layer problem, the expected volume-flux contribution from plume-top entrainment would be a substantial fraction (in the range 0.6–0.8) of the upward volume flux.

To estimate the plume-top entrainment from the LES data, we calculated the absolute ratio of the upward to downward volume fluxes, V_{up}/V_{down}, at z_{max}. The fluxes are relatively small in this region, so to estimate the sensitivity of this result to the height chosen, we calculated the same ratio three grid points below this level. As V_{up}/V_{down} varies with the sample period, in figure 24 we present the mean ratio averaged over typically 3–4 sample periods with error bars representing the standard deviation. The large variation in the magnitude of the error bars between different simulations is due to the small number of available samples. Despite the uncertainty in V_{up}/V_{down}, the numerical results generally show a ratio of $V_{up}/V_{down} \lesssim 0.5$, implying that the entrained volume flux, $V_E = V_{down} - V_{up}$, is at least as much as that in

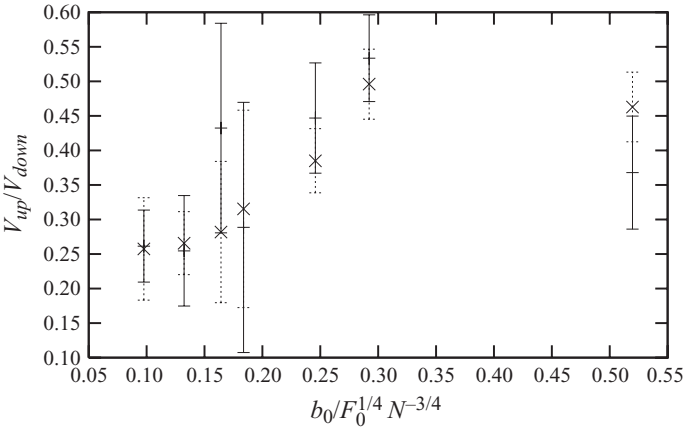

FIGURE 24. The absolute ratio of the upward to downward volume fluxes evaluated at z_{max} (+ with solid error bars) and at the third grid level below z_{max} (× with dotted error bars).

the upward plume. Figure 24 shows the ratio V_{up}/V_{down} tending towards 0.25 as $b_0/F_0^{1/4}N^{-3/4}$ decreases, which gives $V_{down} = 4V_{up}$ or $V_E = 3V_{up}$. Figure 20 shows the ratio V_{down}/V_{up} as a function of height for plume S2. Although V_{down} is large compared with V_{up} at z_{max}, the fluxes themselves are small indicating that the amount of entrained fluid at the plume top may be small despite the large value of V_{down}/V_{up}. Furthermore, below z_{max}, V_{down} increases in magnitude whereas V_{down}/V_{up} decreases. This may be partly due to the cumulative effect of entrainment from both the environment and the upward plume into the downward plume, but is also due to upward moving material overturning and changing direction.

The ratio V_{down}/V_{up} is considerably larger than that observed by Lin & Linden (2005) at a comparable *Ri*. However, as discussed above, our result is obtained from a direct measurement of the upward and downward volumes fluxes at, or near, the top of the plume. Lin & Linden (2005) use a combination of theory and experiment to calculate the entrainment by a fountain impinging on a density interface. The interaction of the fountain with the fluid beyond the interface is not described quantitatively, except for an indication of the vertical extent of penetration beyond that point. This is approximately 0.4 times the distance between the source and the interface for all their experiments. Thus, the entrainment is calculated at a depth of approximately 70 % of the total extent of the fountain. This region is characterized by upward and downward volume fluxes that are much larger than those expected near the maximum extent of the fountain, and corresponds to a region around $z/z_{eq} \approx 1.2$ in our plume S2 (see figure 20). At this height, the ratio V_{down}/V_{up} gives a value of V_E that is closer in magnitude to that observed by Lin & Linden (2005).

These results provide additional information with which to revise the model of BK2000. Assuming that the entrained fluid comes from the maximum height (or overturning height) of the model, the buoyancy flux in the downward plume is unaffected, and the plume-top entrainment can be incorporated by a very simple additional feature. Instead of using the final volume flux from the top of the upward iteration directly as the initial condition for the downward iteration, we use the volume flux increased by a chosen factor to represent the increase due to plume-top entrainment. However, as shown in figure 20, the LES upward and downward volume fluxes are small at z_{max}, and so the inclusion of V_{down} in the initial condition for the

descending plume is unlikely to alter the flow significantly. In the BK2000 model, the process of overturning and direction reversal occurs only at the height at which the momentum flux vanishes but in reality it is likely to occur at a range of heights leading to smoother profiles than the BK2000 model can produce. This means that there is uncertainty in the most appropriate height to diagnose V_E for use in the BK2000 model. Also, although there is a distinction in the BK2000 model, in reality it may be hard to distinguish between entrainment from the upward to the downward plume and material overturning and changing direction. Since the BK2000 plume does not rise as high as the LES plume, we use the value of V_{up}/V_{down} given by the LES data at the level at which the BK2000 plume terminates. For the LES plume S2 this gives $V_{down} = 2V_{up}$ (see figure 20). (With $V_{down} = 4V_{up}$, the downward momentum flux can be made to agree reasonably well with the LES data but the downward volume flux becomes much larger than the downward LES volume flux.) The sharp top of the BK2000 plume then corresponds to the net effect of processes occurring above this point.

We find that, with the revised model, it is possible to produce both volume and momentum fluxes that are similar in magnitude to those observed, provided we tune the entrainment coefficients α, β, γ in the co-flowing region (below the co-flowing region α for the single plume remains at the default value of 0.1). Even with a pre-determined value of plume-top entrainment, the remaining parameter space is still large; however, several trials showed that the best agreement is found with $\alpha, \gamma \ll \beta$ and $\beta \gg 0.147$, its original value. (Adding plume-top entrainment to the model with the original values of α, β and γ results in a downward volume flux that is much larger than the equivalent LES flux.) Physically, this indicates that, with or without plume-top entrainment, detrainment from the upward plume to the downward is more important than vice versa and more important than entrainment from the environment to the downward plume. The upward plume fluid is moving against the buoyancy force upon it in this region, so the preference for detrainment into the downward plume is perhaps not surprising especially as the detrainment process in the model is parameterizing both mixing between the plumes and the bulk overturning and direction reversal. This choice of entrainment coefficients rather than the addition of plume-top entrainment affects the shape of the upward volume flux which now more closely follows the equivalent LES flux. The addition of plume-top entrainment (for given α, β and γ) increases the magnitude of V_{up}, V_{down} and the downward momentum flux, but results in a downward plume that does not penetrate to as great a depth. Physically, the entrainment of warmer fluid above the plume will not only result in an increased volume flux but will also reduce the magnitude of the buoyancy of the downward plume with the result that it will reach equilibrium with the environment at a higher level than is the case with no plume-top entrainment.

The revised BK2000 model with plume-top entrainment and $\alpha = 0.05$, $\beta = 0.8$ and $\gamma = 0.01$ is shown in figures 20 and 21, and the results of this refinement are encouraging. In particular, the final maximum rise height has increased and the positions of the peak values of the upward and downward momentum fluxes are closer to their corresponding LES values. The peak value of the upward volume flux is located closer to its LES counterpart and above this level, the upward volume flux decreases in a manner more similar to the LES upward volume flux than is the case for the original BK2000 model. Without the addition of substantial plume-top entrainment, it was not found possible to capture the behaviour of both the volume and momentum fluxes in this manner. Despite the better agreement with the LES data, there are still substantial differences between the revised BK2000 model

and the LES data. Of course, the LES plume is affected by the finite source size and limited resolution; however, there are features of the BK2000 model that are qualitatively different, such as the downward volume flux. Some of these differences may result from inadequate modelling of the overturning region in the BK2000 model. Additionally, in reality we would expect a further annulus of upward flow beyond the downward shell (and possibly several more upward and downward annuli beyond). This may produce a downward volume flux that decreases with decreasing z below its peak value (i.e. more closely follows the shape of the LES downward volume flux) by providing additional entrainment, detrainment and overturning mechanisms.

An important check on the revised model is its behaviour in the original BK2000 problem of a fountain in a stratified environment. It is found that the same factor of plume-top entrainment (i.e. $V_{down} = 2V_{up}$) and the revised values of the entrainment constants produces results for the plume maximum and final rise heights that are similar to those of BK2000. This indicates that it is possible to introduce plume-top entrainment into the model, and so improve its correspondence with observed behaviour, without reducing its range of applicability.

6. Conclusions

This study set out to make a quantitative comparison of LES of a buoyant plume with the well-known plume equations of MTT. In a uniform environment, the centreline vertical velocity and reduced gravity exhibit the expected scalings sufficiently far above the source. We calculated a value of the entrainment constant, $\alpha = 0.15$, which is consistent with experimental and field measurements, and we found no significant difference in the radial spreading rates of the vertical velocity and reduced gravity. These results indicate that, in a uniform environment, our domain size and resolution are sufficient to mitigate (though not eliminate) the effects of a finite source and produce a well-developed plume that can be compared with a model that assumes a point source.

In a stably stratified environment, the effects of the finite source persist up to the point where the stratification becomes important; not even the smallest value of $b_0/F_0^{1/4}N^{-3/4}$ considered here truly exhibits the expected scalings below the equilibrium level. Nevertheless, a comparison with the plume equations is still warranted: the LES data provide a reasonable solution of the buoyancy and momentum equations throughout the depth of the plume and the volume equation up to the equilibrium level (figures 9–11), justifying the assumptions that underlie the plume equations, such as neglect of the radial pressure gradient (see e.g. Linden 2000, § 3.4); there is reasonable agreement of the LES buoyancy and momentum fluxes with the equivalent MTT and Briggs' model fluxes (see figures 13, 15 and 16); a simple empirical virtual source correction leads to good agreement between the MTT and LES equilibrium levels for all values of $b_0/F_0^{1/4}N^{-3/4}$ (figure 12).

The more sophisticated model of BK2000, which distinguishes between the upward and downward components of the upper plume, captures some aspects of the LES plume though even qualitatively it differs significantly from the LES plume in places. For example, the downward volume flux increases with decreasing z until an abrupt cutoff, whereas the LES downward volume flux decreases smoothly to zero from its peak value. Such flux comparisons are simpler to carry out with LES than in physical experiments such as those of BK2000, who optimized their model for agreement of plume penetration levels. The LES results point to characteristics of buoyant plumes that are, so far, absent from the models of MTT and BK2000: a region of overturning

in which plume-top entrainment plays a role. The inclusion of plume-top entrainment as an additional feature of the BK2000 model, combined with tuning of the co-flowing entrainment parameters (such that together they are a surrogate for the more complicated processes of overturning, entrainment and detrainment that occur near the top of the plume), leads to improved representation of the LES flux profiles and rise heights while maintaining the penetration levels of the original fountain model. However, even this small improvement does not obviate the need for a better model of the overturning region at the top of the plume. This could perhaps be modelled by giving a statistical distribution of plume properties with a corresponding distribution of heights for reversal.

The authors would like to thank Paul Linden for his comments on an earlier version of this manuscript.

Appendix. The BK2000 model

We solve the following dimensionless sets of equations: the upward and downward volume flux (BK2000 (2.11a, b)), the upward and downward momentum flux with the first body-force formulation (denoted by BFI in BK2000, (2.11e, f)) or the second body-force formulation (denoted by BFII in BK2000, (2.11g, h)) and the non-dimensionalized form of the equations for the upward and downward buoyancy flux in a linearly stratified environment (BK2000 (3.1a, b)). Only the second entrainment formulation (denoted by EFII in BK2000), which BK2000 prefer, is considered here.

There is a typographical error in the expression of BK2000 (2.11g) in which the exponent of the term $(1+1/A)$ should be $-1/2$ and not $+1/2$, to match that in (2.11h). The correct sign of the exponent can be obtained only after a moderate amount of algebraic manipulation; however, the fact that the terms should match can easily be verified by comparing the difference between (2.11g) and (2.11h) with the difference between the dimensional equations (2.7) and (2.9).

We use a fourth-order Runge–Kutta method to solve the plume equations. BK2000 solve each of the upward and downward equation sets in turn, terminating when the momentum flux passes through zero (or the downward plume reaches the lower boundary). The output of one cycle is used as forcing for the next cycle in the other direction. Iteration continues until the solutions in each direction are unchanged. An iteration cycle starts with the basic (upward) plume equations (MTT). The mapping of the outflow of the upward plume to the initial conditions of the downward plume was performed by carrying the volume flux over directly and reversing the sign of the buoyancy flux. The momentum flux was also carried over directly, although this is merely to give an initial perturbation, since its value is near zero at this point.

As BK2000 point out, the level of maximum downward penetration may not coincide with the final rise height of the plume, the level at which the plume fluid spreads out. They state that this level may be found approximately by assuming that the downward plume fluid at its maximum penetration rises to the final rise height with no further entrainment. A similar 'zero-entrainment' approximation as a short-cut to the final rise height was applied by Briggs (1984) to the outflow of a basic plume in a stratified environment to estimate the final rise height. BK2000 do not give the formula they use to calculate the final rise height, but it would appear to be derivable in the manner of Briggs (1984). For generality, we consider a forced

plume with initial momentum flux M_0. The ambient density gradient is given by

$$\frac{\mathrm{d}\rho_a}{\mathrm{d}z} = -\frac{\rho_0}{g}\frac{F_0^2}{M_0^2}\sigma,$$

where $\sigma = M_0^2 N^2/F_0^2$ is the dimensionless buoyancy frequency. Hence, the dimensionless reduced gravity of the downward plume, $\tilde{g}'_d = \overline{g'}_d/(M_0^{-5/4}F_0^{3/2})$, becomes

$$\tilde{g}'_d = M_0^{5/4}F_0^{-3/2}g\frac{(\rho_d - \rho_0)}{\rho_0} + \sigma\tilde{z},$$

where $\tilde{z} = M_0^{-3/4}F_0^{1/2}z$ and ρ_0 is the ambient density at the lower boundary. At the level of maximum downward penetration

$$\rho_d(\tilde{z}_{mdp}) = \rho_0(1 + g^{-1}M_0^{-5/4}F_0^{3/2}(\tilde{g}'_d(z_{mdp}) - \sigma\tilde{z}_{mdp}))$$

and the final rise height is given by solving $\rho_a(\tilde{z}_{final}) = \rho_d(z_{mdp})$. This yields the simple relationship

$$\tilde{z}_{final} = \tilde{z}_{mdp} - \frac{\tilde{g}'_d(z_{mdp})}{\sigma}.$$

Since the dimensionless reduced gravity is negative at the level of maximum downward penetration, having overshot the equilibrium level on the way down, it can be seen that $\tilde{z}_{final} > \tilde{z}_{mdp}$ as expected. In the case where the downward plume reaches the lower boundary, the correction is calculated in the same manner if necessary.

BK2000 developed their model for a turbulent fountain with non-zero initial momentum and buoyancy fluxes. For a pure plume, $M_0 = 0$, so it is necessary to follow the MTT convention of non-dimensionalizing using F_0 and N. The equations are effectively the same, except that we replace M_0 by F_0/N in the non-dimensionalization. For this non-dimensionalization, it follows that the only case to study is that of $\sigma = 1$.

With BFII the initial plume did not rise as high as the final plume. The method of solution had to be adapted in this case to accommodate the momentum flux in the inner plume not tending to zero at the initial maximum rise height. This was done by using the fluxes at the end of the inner-plume cycle to initialize a solution of the simple-plume equations, and the concatenation of these two solutions was then used as forcing for the outer plume.

REFERENCES

Abdalla, I. E., Cook, M. J., Rees, S. J. & Yang, Z. 2007 Large-eddy simulation of buoyancy-driven natural ventilation in an enclosure with a point heat source. *Intl J. Comput. Fluid Dyn.* **21**, 231–245.

Akselvoll, K. & Moin, P. 1996 Large-eddy simulation of turbulent-confined coannular jets. *J. Fluid Mech.* **315**, 387–411.

Baines, W. D. & Turner, J. S. 1969 Turbulent buoyant convection from a source in a confined region. *J. Fluid Mech.* **37**, 51–80.

Bastiaans, R. J. M., Rindt, C. C. M., Nieuwstadt, F. T. M. & van Steenhoven, A. A. 2000 Direct and large-eddy simulation of the transition of two- and three-dimensional plane plumes in a confined enclosure. *Intl J. Heat Mass Transfer* **43**, 2375–2393.

Bloomfield, L. J. & Kerr, R. C. 2000 A theoretical model of a turbulent fountain. *J. Fluid Mech.* **424**, 197–216.

Briggs, G. A. 1975 Plume rise predictions. In *Lectures on Air Pollution and Environmental Impact Analyses* (ed. D. A. Haugen), pp. 59–111. American Meteorological Society.

Briggs, G. A. 1984 Plume rise and buoyancy effects. In *Atmospheric Science and Power Production* (ed. D. Randerson), pp. 327–366. Office of Research, US Department of Energy.

Cardoso, S. S. S. & Woods, A. W. 1993 Mixing by a turbulent plume in a confined stratified region. *J. Fluid Mech.* **250**, 277–305.

Devenish, B. J. & Edwards, J. M. 2009 Large-eddy simulation of the plume generated by the fire at the Buncefield oil depot in December 2005. *Proc. R. Soc. Lond.* A **465**, 397–419.

George, W. K., Alpert, R. L. & Tamanini, F. 1977 Turbulence measurements in an axisymmetric buoyant plume. *Intl J. Heat Mass Transfer* **20**, 1145–1154.

Gupta, A. K. 1993 Fire plume: theories and their analysis. *J. Appl. Fire Sci.* **2**, 269–298.

Hunt, G. R. & Kaye, N. G. 2001 Virtual origin correction for lazy turbulent plumes. *J. Fluid Mech.* **435**, 377–396.

Kantha, L. H. & Clayson, C. A. 2000 *Numerical Models of Oceans and Oceanic Processes*. Academic Press.

Leonard, B. P., Lock, A. P. & MacVean, M. K. 1996 Conservative explicit unrestricted-time-step multidimensional constancy-preserving advection schemes. *Mon. Weather Rev.* **124**, 2588–2606.

Lin, Y. J. P. & Linden, P. F. 2005 The entrainment due to a turbulent fountain at a density interface. *J. Fluid Mech.* **542**, 25–52.

Linden, P. F. 2000 Convection in the environment. In *Perspectives in Fluid Dynamics* (ed. G. K. Batchelor, H. K. Moffat & M. G. Worster), pp. 289–345. Cambridge University Press.

List, E. J. 1982 Turbulent jets and plumes. *Annu. Rev. Fluid Mech.* **14**, 189–212.

Manins, P. C. 1973 Confined convective plumes. PhD thesis, University of Cambridge, Cambridge.

Manins, P. C. 1979 Turbulent buoyant convection from a source in a confined region. *J. Fluid Mech.* **91**, 765–781.

Mason, P. 1989 Large-eddy simulation of the convective atmospheric boundary layer. *J. Atmos. Sci.* **46**, 1492–1516.

McDougall, T. J. 1981 Negatively buoyant vertical jets. *Tellus* **33**, 313–320.

Morton, B. R. 1959 Forced plumes. *J. Fluid Mech.* **5**, 151–163.

Morton, B. R., Taylor, G. & Turner, J. S. 1956 Turbulent gravitational convection from maintained and instantaneous sources. *Proc. R. Soc. Lond.* A **234**, 1–23.

Nieuwstadt, F. T. M. & de Valk, J. P. J. M. M. 1987 A large eddy simulation of buoyant and non-buoyant plume dispersion in the atmospheric boundary layer. *Atmos. Env.* **21**, 2573–2587.

Pasquill, F. & Smith, F. B. 1983 *Atmospheric Diffusion*. Ellis Horwood.

Pham, M. V., Plourde, F. & Doan, K. S. 2007 Direct and large-eddy simulations of a pure thermal plume. *Phys. Fluids* **19**, 125103.

Piacsek, S. A. & Williams, G. P. 1970 Conservation properties of convection difference schemes. *J. Comput. Phys.* **6**, 392–405.

Plourde, F., Pham, M. V., Kim, S. D. & Balanchandar, S. 2008 Direct numerical simulations of a rapidly expanding thermal plume: structure and entrainment interaction. *J. Fluid Mech.* **604**, 99–123.

Le Ribault, C., Sarkar, S. & Stanley, S. A. 1999 Large eddy simulation of a plane jet. *Phys. Fluids* **11**, 3069–3083.

Rooney, G. G. & Linden, P. F. 1996 Similarity considerations for non-Boussinesq plumes in an unstratified environment. *J. Fluid Mech.* **318**, 237–250.

Scase, M. M., Caulfield, C. P. & Dalziel, S. B. 2006 Boussinesq plumes and jets with decreasing source strengths in stratified environments. *J. Fluid Mech.* **563**, 463–472.

Turner, J. S. 1973 *Buoyancy Effects in Fluids*. Cambridge University Press.

Turner, J. S. 1986 Turbulent entrainment: the development of the entrainment assumption, and its application to geophysical flows. *J. Fluid Mech.* **173**, 431–471.

Yan, Z. H. 2007 Large-eddy simulations of a turbulent thermal plume. *Heat Mass Transfer* **43**, 503–514.

Zhou, X., Luo, K. H. & Williams, J. J. R. 2001 Large-eddy simulation of a turbulent forced plume. *Eur. J. Mech.* B. *Fluids* **20**, 233–254.